IEEE Access
Multidisciplinary | Rapid Review | Open Access Journal

Received May 18, 2018, accepted June 26, 2018, date of publication July 5, 2018, date of current version August 15, 2018.

Digital Object Identifier 10.1109/ACCESS.2018.2853150

Spectral Mapping Based on Panchromatic Block Structure Analysis

XIAOYAN LUO[1], (Member, IEEE), LIANGYU ZHOU[1], XIAOFENG SHI[2], HAN WAN[3], AND JIHAO YIN[1], (Senior Member, IEEE)

[1]School of Astronautics, Beihang University, Beijing 100191, China
[2]School of Electronic and Information Engineering, Beihang University, Beijing 100191, China
[3]School of Computer Science and Engineering, Beihang University, Beijing 100191, China

Corresponding author: Xiaofeng Shi (shixiaofeng@buaa.edu.cn)

This work was supported in part by the National Key Research and Development Program of China under Project 2018YFB0505100 and in part by the National Natural Science Foundation of China under Grant 41471278.

ABSTRACT Fusing panchromatic (PAN) and multispectral (MS) images, i.e., pansharpening, can obtain a high-resolution MS (HRMS) image. In this paper, we propose a spectral mapping framework for pansharpening problem based on PAN block structure analysis (PBSA). The PBSA employs boundary, inner uniqueness, and neighborhood comparisons as block structure characteristics to classify the PAN image blocks into pureness composition and mixture composition. For the PAN blocks with pureness composition, they can directly copy the spectral information of corresponding MS pixels. For the mixture PAN blocks, assuming that they can linearly represented by some pure PAN blocks, their spectral signals can get via a weighted average from the relative pure PAN blocks. The experiments on real PAN and MS pairs show that the proposed pansharpening method not only conforms to the structure of the PAN image but also preserves the spectral information of the MS image. The final fused HRMS image shows good performance in visual effect and objective assessment.

INDEX TERMS Remote sensing, image fusion, pansharpening.

I. INTRODUCTION

The current optical satellites can simultaneously capture panchromatic image (PAN) and multispectral image (MS) [1]. Because of the platform limitation, they have complementary characteristics in spatial and spectral domains, i.e., high-resolution PAN image and low-resolution MS image (LRMS). To generate an enhanced high-resolution multispectral image (HRMS), many remote sensing applications combine the PAN and LRMS images together via a pansharpening technique [2]–[4].

As an important research branch of image fusion, pansharpening technique aims at injecting the spatial detail of PAN image into MS to produce HRMS images. Therefore, most classical pansharpening algorithms share a unique framework comprising of two sequential phases: 1) extracting the spatial details from PAN image and 2) injecting the extracted details into the MS image [5]–[7]. They can be mainly divided into two categories: component substitution (CS) and multiresolution analysis (MRA). To convert the upsampled MS image into spatial and spectral details, the CS-based methods are based on a decorrelation transform, while the MRA-based approaches draw support from a multiresolution decomposition.

For CS-based methods, earlier researchers convert the upsampled MS image into independent components of intensity–hue–saturation (IHS) color system and then directly use PAN image to replace I component [8], [9]. However, the simple IHS transform only fits color image with red, green and blue three channels. To obtain I component for MS images with more than three channels, a generalized IHS (GIHS) method has been proposed via averaging MS channels with the additional near-infrared (NIR) channel or multispectral [10]. Simply, it captures the spatial detail by calculating the difference value between I component and PAN image [10]. In fact, if the difference value is large, the IHS technique often brings spectral distortions. To overcome this problem for IHS fusion, Choi considers the minimization problem of spectral distortion, and uses a parameter to control the tradeoff between the spatial and spectral resolution of fused image [11]. Tu *et al.* integrate a simple spectral response modification into a fast IHS method to develop a spectral-adjusted scheme [12],

2169-3536 © 2018 IEEE. Translations and content mining are permitted for academic research only.
Personal use is also permitted, but republication/redistribution requires IEEE permission.
See http://www.ieee.org/publications_standards/publications/rights/index.html for more information.

and also present a tunable IHS-Brovey method preserving spectral characteristics [13]. To improve the spectral quality, a nonlinear IHS method (NIHS) [14], an adaptive IHS method [15], and a spatially adaptive IHS method [16] are proposed. To improve the adaptive IHS fusion, Leung *et al.* design a more adaptive weighting matrix in the spatial detail injection step [17]. Similar to the IHS transform, principal component analysis (PCA) transform has been popularly used for pansharpening. González-Audícana *et al.* replace the first principal component by PAN image [18]. Shah *et al.* merge the adaptive PCA and contourlet transform to reduce the spectral distortion [19]. As a generalization of PCA, Gram–Schmidt (GS) transformation is used to define a powerful pansharpening method [20]. Based on image segmentation, the region-dependent injection coefficients are applied to GS orthogonalization procedure [21].

On the other hand, the MRA-based pansharpening model obtains spatial details through a multiresolution decomposition method, such as the discrete wavelet transform [22]–[24], the wavelet frames [25], the Laplacian pyramid [26], and the curvelet transform [27]. In addition, the generalized Laplacian pyramid (GLP) method [28] has been widely used in pansharpening community, in which the corresponding differential representation is estimated by calculating the differences between the Gaussian pyramid levels. The GLP with the modulation transfer function (MTF)-tailored filter (MTF-GLP) can extract the invisible details in MS but existing in PAN image when the frequency response of filter matches the corresponding sensor MTF [29]. Taking the local varieties of injection coefficient into account, the MTF-GLP with context based decision (MTF-GLP-CBD) is proposed [30]. In practice, the implementation of MRA relies on filtering operation, which could produce ring artifacts and then reduce the visual quality of fusion image.

Based on the improvement of some optimization techniques, many pansharpening methods for MS and PAN images are proposed. For instance, the band-dependent spatial-detail (BDSD) method estimates spatial details by the minimum mean-square-error (MMSE) [31]. For a better spectral content preservation, a generalized version of BDSD is proposed [32]. With a pair of low and high resolution dictionaries, the fused image is obtained from sparse reconstruction [33], [34]. Considering that MS channels have a common low-rank component, a joint sparse and low-rank decomposition is employed for pansharpening of multispectral images [35]. Masi *et al.* [36] and Wei and Yang [37] apply deep learning in pansharpening processing. All these methods obtain a very good performance against a number of traditional pansharpening methods, but the computation burden on optimization strongly limits its practical application [38].

In sum, the most existing pansharpening methods aim to preserve the spatial information of PAN image and minimize spectral distortions, in which upsampling operation is necessary to extract the spatial detail. However, upsampling process ignores the spatial structure existing in PAN image, so it could lead to spatial structure inaccuracy and followed spectral aliasing distortions inescapably. For some pixels located at the edges of objects, their spectral information in LRMS image is mixed by different materials which can be easily observed in correspond high resolution PAN blocks. Therefore, making use of the PAN structure is a good selection to improve the spatial and spectral accuracy.

In this paper, we propose a spectral mapping framework for pansharpening problem based on panchromatic block structure analysis (PBSA). According to the structure analysis in terms of boundary, inner uniqueness and neighborhood characteristics, the PAN image blocks and their corresponding LRMS pixels are categorized into pureness composition and mixture composition classes. For pure LRMS pixels, their spectral information is directly mapping to their high resolution PAN blocks. To capture correct spectral information for mixed pixels, we adopt pixel-based weighted mapping manner in corresponding mixed PAN blocks. Furthermore, to reduce the spatial information influence of spectral mapping, a simple intensity modification is applied to HRMS with reference to PAN. Under the precise guidance of PAN structure, not only the spatial characteristics of the PAN image is preserved, but also the pure spectral information is completely remained and the mixed one is efficiently constructed. Thus, our proposed PBSA-based spectral mapping can acquire a better perceptive performance for the pansharpened image.

The remainder of this paper is structured as follows. In Section II, details of our proposed algorithm are introduced in two parts of class categorization and spectral mapping. The effectiveness of the proposed method is demonstrated in Section III by experimental results on real MS and PAN image pairs. Finally, Section IV gives the conclusion of this paper and suggests some future researches.

II. OUR PROPOSED METHOD

In this section, we propose a PBSA-based spectral mapping algorithm for LRMS and PAN image fusion. To simplify the explanation, we assume that the original LRMS and PAN images have been registered. As depicted in Fig. 1, the algorithm begins with class categorization of pure or mixed compositions for PAN blocks and LRMS pixels, because the spectral information in high spatial resolution is strongly related to the material composition of the scene objects. Referring to the composition partition, the spectral signal of HRMS pixels can be mapped by two distinguished strategies. Finally, the fused HRMS image is modified by using the intensity difference with PAN image. In the following sections, the operations are explained in detail.

A. PANCHROMATIC BLOCK STRUCTURE PROPERTY

As previously mentioned, many pansharpening methods firstly get HRMS from LRMS via independent upsampling step, and then inject spatial detail of PAN image into HRMS. However, the upsampling without PAN structure knowledge can cause spectral distortion, especially for those mixed pixels which contain more than one material. To obtain an

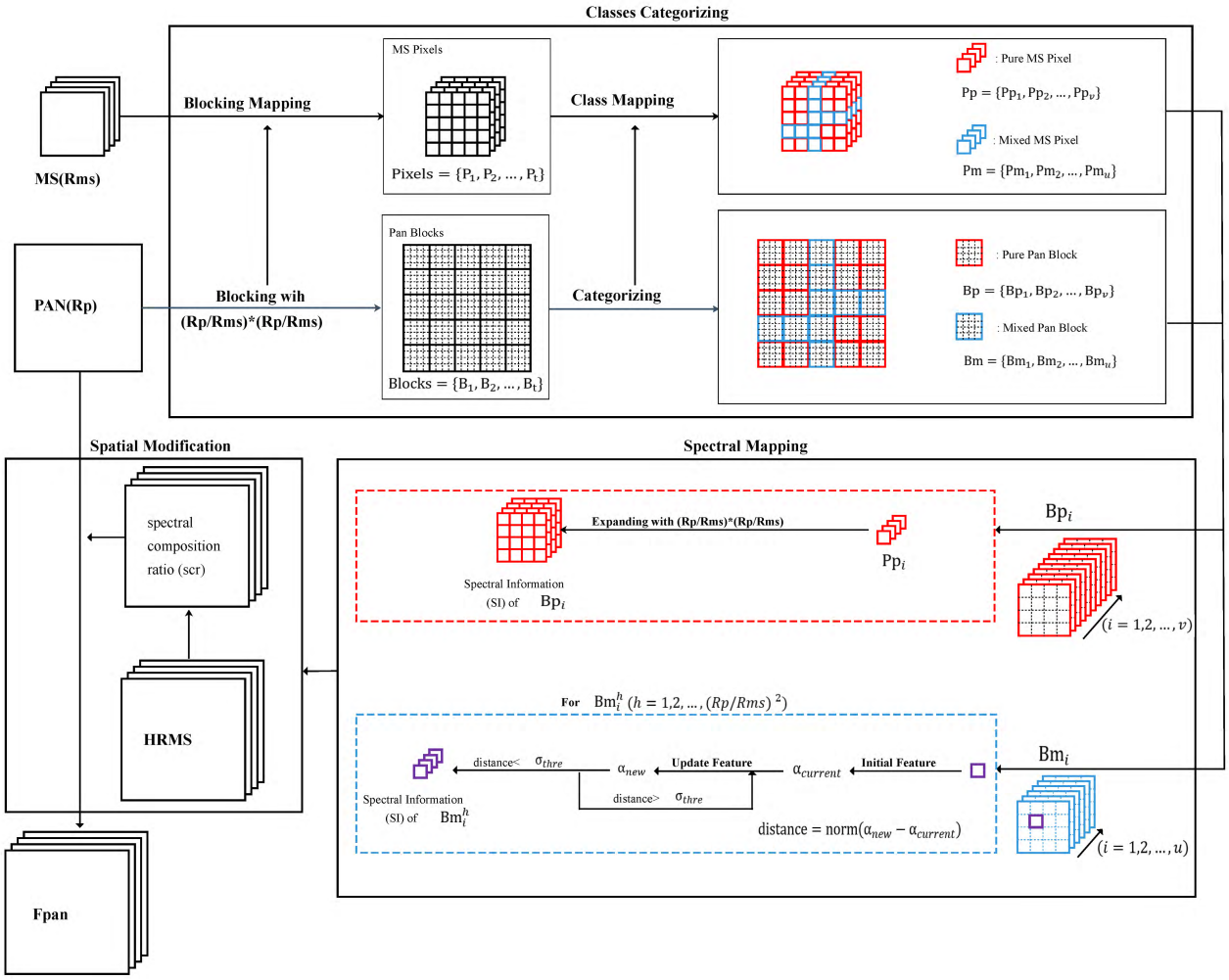

FIGURE 1. Flowchart of PBSA-BASED pansharpening method.

HRMS with consistent spectral information and spatial structure, we first focus on structure analysis of PAN block to aid spectral mapping from LRMS pixel to PAN block.

To understand whether the PAN block is pure composition or mixed composition, we first investigate what a pure composition structure is in PAN blocks. In computer vision, objects in an image are defined via characterizing by a well-defined boundary in space, sometimes uniqueness within the image, and a different appearance from their surrounding [39]. Inspired by this, boundary, inner uniqueness and comparison with neighbors are considered to define a pure composition structure for a PAN block. Intuitively, edge is viewed as a boundary of many objects, so a PAN block without any edge point could be regarded as potential pure blocks of one material. To filter out the mixed blocks from the candidate pure blocks, we utilize the standard deviation of the one PAN block to denote its inner unique homogeneity, and the distance comparison with 4 neighbor blocks is used to define the different appearance of block object from the surrounding.

B. PANCHROMATIC BLOCK CLASS CATEGORIZATION

For one L-band LRMS and PAN image pair with spatial resolutions $Nms = Rms \times Rms$ and $Npan = Rpan \times Rpan$ respectively, their spatial resolution ratio is $r = Rpan/Rms$. To keep LRMS pixel as operated unit, we divide the PAN image into blocks with size of $r \times r$. After that, all LRMS pixels $\mathbf{P} = \{Pi, i = 1, \ldots, Nms\}$ can be corresponded to PAN blocks in $\mathbf{B} = \{\mathbf{Bi}, i = 1, \ldots, Nms\}$. For the same region, the MS pixel denotes the spectral integration, and the PAN block shows the spatial structure information. Since the spatial structure decides the spectral integration, the classification of PAN block structure can improve their spectral mapping results.

For a PAN block, if there exist less edge points, it is potential to be pure composition. Given ne indicating the number of points existing edge, $ne < \tau_e$ means this block is potential pure block.

Using $\mathbf{Bi} = \{P_{bi}, bi = 1, \ldots, Nb\}$ to indicate the $Nb = r \times r$ PAN pixels in this block, its inner uniqueness can be measured by their change dispersion, which can be

formulated in standard deviation as follows.

$$sp = \sqrt{\frac{1}{Nb}\sum_{bi=1}^{Nb}(P_{bi} - \bar{a})^2}, \quad \bar{a} = \frac{1}{Nb}\sum_{bi=1}^{Nb} P_{bi} \tag{1}$$

The smaller sp means that the block pixels change more slightly. Given a small threshold parameter τ_s, if $sp < \tau_s$, the PAN block **Bi** should be pure block candidate.

Usually, the different appearance property of one block can be obtained via comparing its spectral information with its MS pixel neighbors. Assuming that the corresponding MS pixel of block **Bi** is Pi and its MS spectral vector is $\mathbf{MS}(Pi)$, the related LRMS neighbor pixels are $\mathbf{N_{Pi}} = \{Pnj, nj = 1, 2, 3, 4\}$. The different appearance property of PAN block can be defined as the corresponding spectral distance summary in LRMS.

$$dms = \sum_{j=1}^{4} \|\mathbf{MS}(Pi) - \mathbf{MS}(Pnj)\|_2 \tag{2}$$

where $\|\cdot\|_2$ denotes the 2-norm operator. If the different appearance index is small enough, i.e. $dms < \tau_d$, the corresponding PAN block is regarded as holding monochromatic characteristic.

According to the structure analysis, we can get PAN block structure parameters, i.e. edge number ne, uniqueness property sp, and appearance property dms. Comparing with three thresholds $\{\tau_e, \tau_s, \tau_d\}$, we can distinguish them as pure composition block subset $\mathbf{Bp} = \{\mathbf{Bp_1}, \ldots, \mathbf{Bp_i}, \ldots, \mathbf{Bp_v}\}$ and mixed block subset $\mathbf{Bm} = \{\mathbf{Bm_1}, \ldots, \mathbf{Bm_i}, \ldots, \mathbf{Bm_u}\}$. Correspondingly, the LRMS pixels can be partitioned into pure pixel subset $\mathbf{Pp} = \{Pp_1, \ldots, Pp_i, \ldots, Pp_v\}$ and mixed pixel subset $\mathbf{Pm} = \{Pm_1, \ldots, Pm_i, \ldots, Pm_u\}$.

C. SPECTRAL MAPPING SCHEMES

Considering that one pure composition structure PAN block includes stable pixels inside the covering region, they have similar or even same spectral information to the corresponding pixel in LRMS. Therefore, the pixel spectral signal in LRMS can directly remain to the corresponding locations in PAN blocks as HRMS regions. For the mixed composition PAN blocks, we assume that they are integrated some pure blocks in the same image, and then their spectral information can be captured via weighting in according with the similarity comparison to related pure PAN blocks. Therefore, we introduce two discriminatory spectral mapping schemes here.

For a pure PAN block $\mathbf{Bp_i}$, its pixels can be regarded as the same material, and then no matter its corresponding LRMS pixel or HRMS block pixels could represent similar spectral information. Therefore, the spectral vector in HRMS pixels limited in PAN block $\mathbf{Bp_i}$ can directly duplicate from the spectral vector $\mathbf{MS}(Ppi)$ of LRMS pixel Pp_i. If the location set of PAN block $\mathbf{Bp_i}$ is denoted as $\Lambda_{Bpi} = \{(x, y) : x = 1, \ldots, r; y = 1, \ldots, r\}$, the HRMS spectral can be obtained from the following formula.

$$\mathbf{HRMS}(x, y) = \mathbf{LRMS}(Ppi), \quad (x, y) \in \Lambda_{Bpi} \tag{3}$$

In the contrast, a mixed PAN block $\mathbf{Bm_i}$ composes of different materials, so its corresponding HRMS pixels could represent respective spectral information. On the other hand, the LRMS pixel Pm_i integrates multiple classes of spectral information. Therefore, it is questionable to estimate the spectral information of HRMS block pixels from its mixed LRMS pixel Pm_i. Considering that the objects have structural repeatability in remote sensing, it is a good alternative to seek the original pure spectral information for the mixed pixels. Owing to the detailed information of PAN blocks, we find the similar pure blocks of mixed block around its limited neighbor regions. Centered at mixed PAN block $\mathbf{Bm_i}$, its neighborhood is windowed in the $W \times W$, and $W > 3r$ is constrained to make the neighbor regions effective.

The following steps explain the spectral mapping process for mixed block $\mathbf{Bm_i}(i = 1, \ldots, u)$.

Step 1: Initialize the HRMS spectral information of $\mathbf{Bm_i}$ via average of estimated spectral information in most similar pure PAN blocks. From the pure PAN blocks. Nr PAN blocks are found with smallest absolute distance of mean difference to the mixed block. The initial estimated HRMS spectral signal for this block can be captured from the following formula.

$$\mathbf{HRMS}(x, y) = \frac{1}{Nr}\sum_{j=1}^{Nr}\mathbf{LRMS}\left(Pp_j\right), \quad (x, y) \in \Lambda_{Bmi} \tag{4}$$

where Pp_j $(j = 1, \ldots, Nr)$ are the corresponding LRMS pure pixels to the Nr most similar PAN blocks.

Step 2: Calculate some features to represent each pure PAN block $\mathbf{Bp_i}$, including the PAN intensity mean value $(\bar{a})$, corresponding LRMS spectral vector $(\mathbf{LRMS}(Pp_i))$, and the minimal local binary pattern $(\min(lbp(\Lambda_{Bpi})))$ in PAN block.

Step 3: Calculate same features for each pixel in mixed PAN block $\mathbf{Bm_i}$, including the PAN intensity $(p(x, y))$, HRMS spectral vector $(\mathbf{HRMS}(x, y))$, and local binary pattern $(lbp(x, y))$ in PAN block.

Step 4: Compare each mixed PAN pixel feature $\mathbf{fP} = [p(x, y), \mathbf{HRMS}(x, y), lbp(x, y)]$ with the feature $\mathbf{fB} = [\bar{a}, \mathbf{LRMS}(Pp_i), \min(lbp(\Lambda_{Bpi}))]$ of all pure PAN blocks in Euclidean distance.

For one mixed pixel $Pj = (x, y) \in \Lambda_{Bmi}$, its Euclidean distance of the feature vector to $\mathbf{Bp_i}$ is defined as

$$dfi = \|\mathbf{fPj} - \mathbf{fBi}\|_2, \quad i = 1, \ldots, v \tag{5}$$

Step 5: Find Nr pure blocks with smallest Euclidean distance of the feature vector to update the HRMS spectral information of $\mathbf{Bm_i}$, according to the similarity weighted. According to the distance factor adjusting, the HRMS spectral signal for this mixed pixel can be updated by weighted average from pure LRMS spectral vector of the corresponding to the Nr most similar pure PAN blocks.

$$\mathbf{HRMS}(x, y) = \frac{1}{\sum_{i=1}^{Nr} dfi}\sum\nolimits_{j=1}^{Nr}[dfi \cdot \mathbf{LRMS}\left(Pp_j\right)] \tag{6}$$

Step 6: Repeat from Step 3.

D. SPATIAL MODIFICATION

Referring to the PAN structure analysis, the HRMS is estimated via direct spectral mapping or indirect spectral synthetizing. Unavoidably, the PAN structure could be influenced more or less. To furthermore maintain the spatial details of PAN image, we modify the estimated HRMS image via the simplest approximation of PAN with spectral composition ratio (scr) to obtain the final fusion pansharpened image.

For one pixel at location (x, y) and spectral channel b in spatial image $Rp \times Rp$, the final HRMS spectral information $Fpan$ at location (x, y, b) can be modified by formula (7).

$$\begin{cases} scr\,(x, y, b) = HRMS\,(x, y, b) \,/\, \dfrac{\sum_{b=1}^{L} HRMS\,(x, y, b)}{\mathrm{L}} \\ Fpan\,(x, y, b) = scr(x, y, b) \cdot PAN(x, y) \end{cases} \tag{7}$$

where L represents the number of multiple spectral bands, $scr(x, y, b)$ denotes each spectral composition ration to averaged value.

E. THE ALGORITHM

To explain our method more understandably, the pseudocode for the main parts is described as follows.

Algorithm 1 The Proposed Pansharpening Algorithm.

Input: Registered PAN and LRMS image pair.
Output: The fusion image with both high spatial and spectral resolution *Fpan*.
Initialize: Empirically, the thresholds for the properties of pure PAN block are set as $\tau_e = 0$, $\tau_s = 20$, $\tau_d = 40$, and the parameters for mixed pixel spectral mapping are given as $W = 15$, Nr=4.

```
Rms = size (LRMS) , Rp = size (PAN) , r = Rp/Rms
Emap = Edge(PAN)
Fmap = LBP(PAN)
B = {Bi, i = 1, . . . , Rp/r} = Block(PAN, r)
for each block Bi (i = 1, 2, . . . , Rp/r) do
    ne ← Emap(Bi)
    if ne ≤ τe then sp ← fomula (1)
      if sp < τs then dms ← formula(2)
          if dms < τd then Bp ← Bi
           else Bm ← Bi
       else Bm ← Bi
    else Bm ← Bi
end for
 for each pure block Bpi do
     HRMS(Bpi) ← formula(3)
 end for
 for each mixed block Bmi do
     HRMS (Bmi) ← step 1 − 6 with iterations
end for
for each HRMS pixel
     Fpan (x, y, b) ← formula(7)
 end for
 Output ← Fpan
```

III. EXPERIMENTS

Our PBSA-based method improves spectral interpolated performance of LRMS with the aid of PAN structure analysis and remains the spatial detail of PAN image. Based on these two aspects, we evaluate the performance of our method on the well registered LRMS-PAN image pairs captured from practical scene. We select CS-based IHS, PCA, Brovey, PRACS, optimization-based BDSD, MRA-based ATWT, and AWLP, MTF-GLP, MTF-GLP-CBD to compare, which can be can found at an available Pansharpening Tool in [6]. Also, two recent NIHS [14] and MF [40] methods are included in the experiments. For all these state-of-the-art algorithms, the LRMS image is required to be interpolated to the spatial size of PAN image. Here, we use a unified cubic interpolation to obtain the upsampled HRMS image, and then perform the parsharpening fusion operations.

The comparisons are tested on two recent high-resolution satellite images of GeoEye-1. They have four 2.0m resolution spectral bands (blue, green, red and near IR) and 0.5m resolution of PAN image. All experiments are implemented on a PC with Intel Core 2 Duo 2.30 GHz CPU and 3GB RAM, and the simulation software is Matlab.

A. VISUAL COMPARISON

To evaluate the visual performance with other pansharpening methods in remote sensing, we select some regions covering different objects as test datasets [41]. Especially, Fig. 2 has one white roof of large building and town background in city, and Fig. 3 holds a main road including several cars in the center. Fig. 2 and Fig. 3 show the pansharpened results in RGB bands for the PAN-LMRS fusion algorithms.

As shown in Fig. 2, because of the beginning with simple interpolated HRMS image, the complex structure regions of grass and tree generate blurring in final pansharpened images. Especially, we can observe from the partial enlargement view, our performance better for the black and white grid at roof edge, the texture of uneven lawn, the complex branch and shadow of trees than other compared methods.

Similarly, owing to the sequel influence of first independent upsampling, the regions covering edge structures are blurred in Fig. 3 (b), Fig. 3(e), and Fig. 3(f) $\sim$ Fig. 3(n). Taking an example at the region marked by a red rectangular box in Fig. 3, the car can capture white color in all pansharpening methods. However, all the compared methods generate blurred edge around the car. In particular, the color diffusion in Fig. 3(b) causes the color aliasing at the joint regions between white car and grey road in Fig. 3(f) $\sim$ Fig. 3(n).

Benefitting from the structure-driven, our PBSA-based method can remain the PAN structure characteristics on spectral mapping. That is to say, the PAN structure information, which can aid the spectral composition analysis of LRMS to guide the spectral. Therefore, our method generates good results than any other methods in structure and multiple spectral fusion.

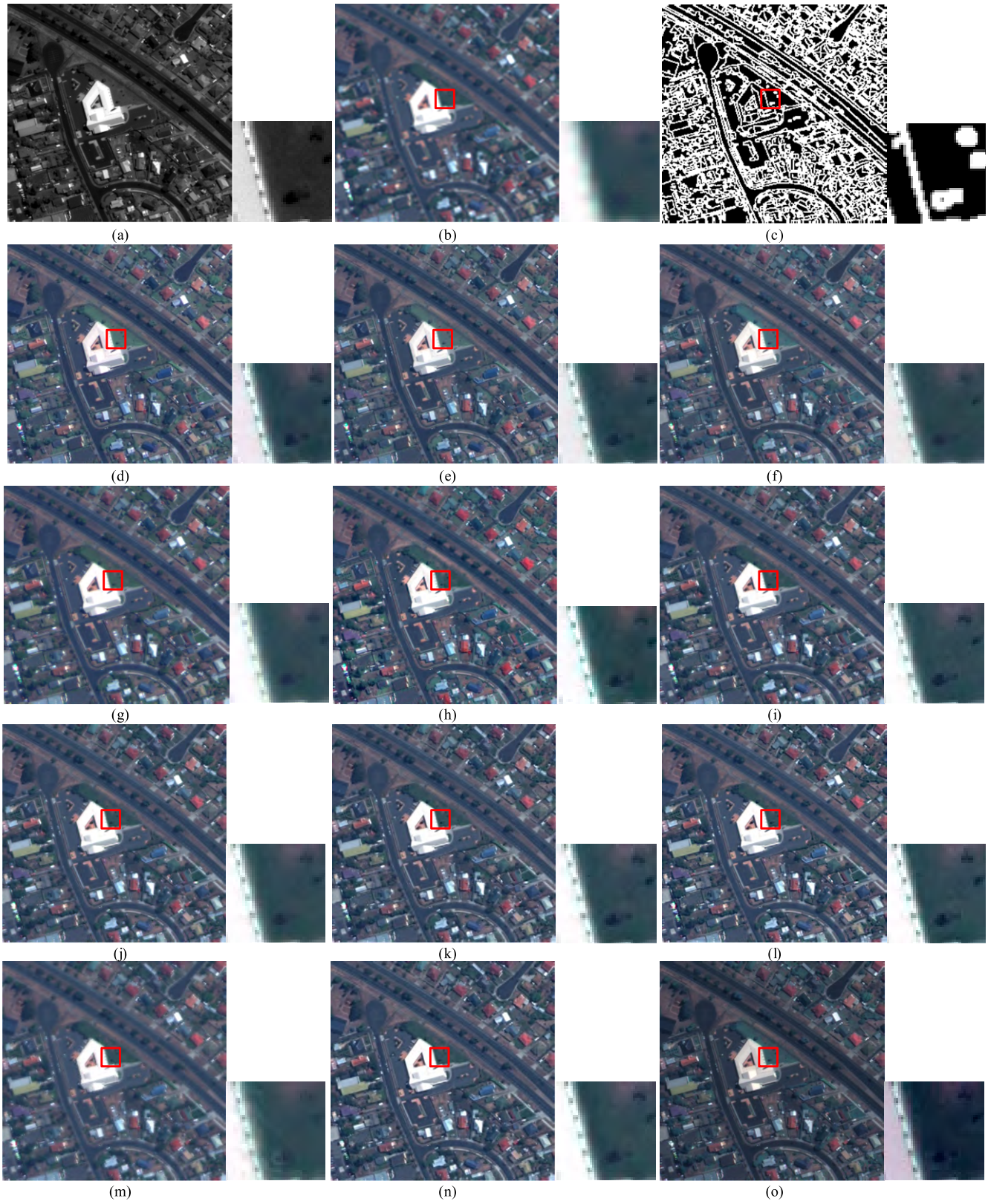

FIGURE 2. The pansharpened images shown with R-G-B band of different fusion methods for GeoEye-1 data, and the detail view of selected regions by red rectangular box at location (x=230, y=205) with 40 pixel length and width. (a) Original PAN. (b) Upsampled MS. (c) Edges of PAN. (d) IHS. (e) PCA. (f) Brovey. (g) PRACS. (h) BDSD. (i) ATWT. (j) AWLP. (k) MTF-GLP. (l) MTF-GLP-BCD. (m) NIHS. (n) MF. (o) Our PBSA-based.

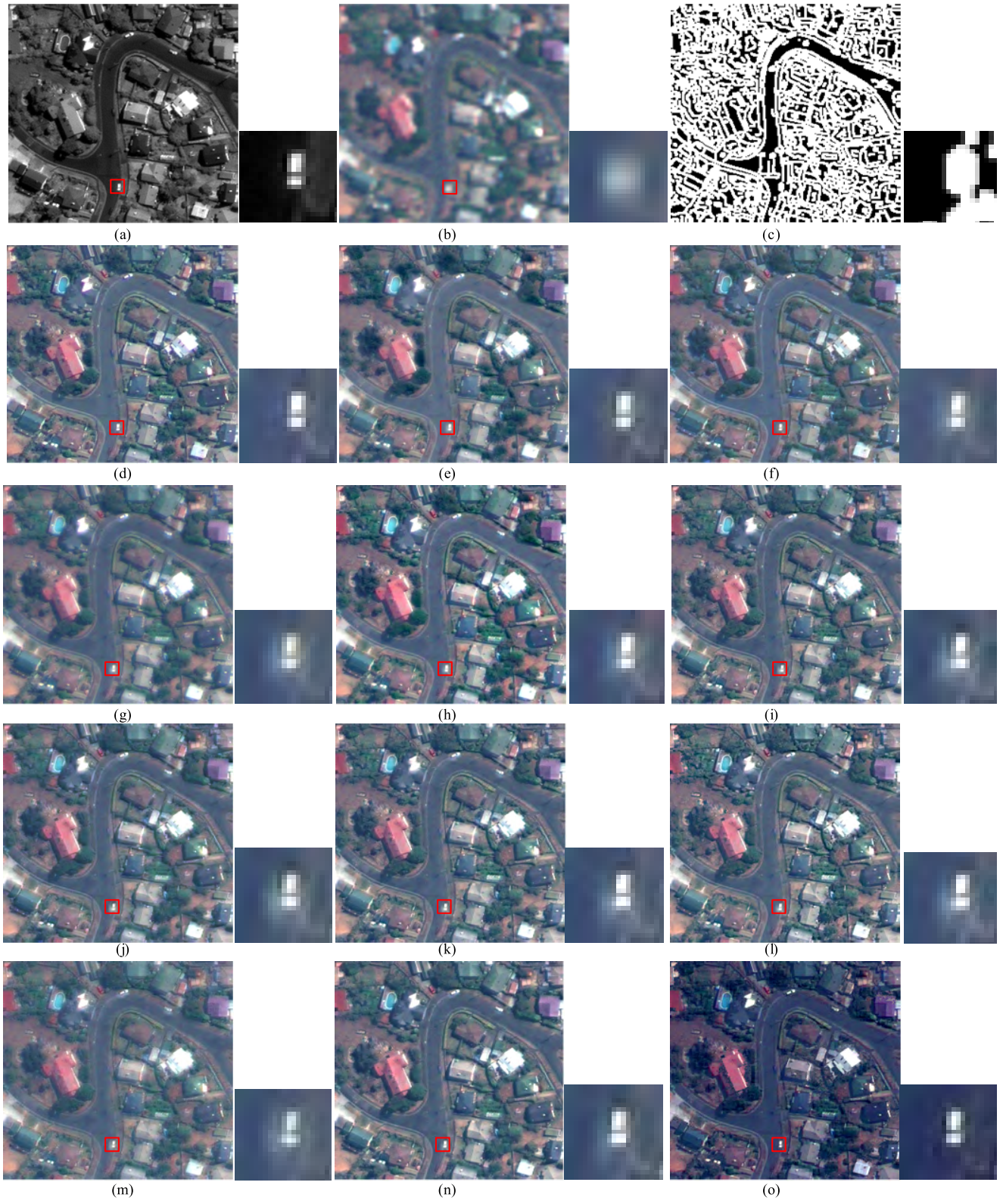

FIGURE 3. The pansharpened results showing with R-G-B band of different fusion methods for GeoEye-1 data, and the detail view of selected regions by red rectangular box at location (x=114, y=198) for 20 pixel length and width. (a) Original PAN. (b) Upsampled MS. (c) Edges of PAN. (d) IHS. (e) PCA. (f) Brovey. (g) PRACS. (h) BDSD. (i) ATWT. (j) AWLP. (k) MTF-GLP. (l) MTF-GLP-BCD. (m) NIHS. (n) MF. (o) Our PBSA-based.

TABLE 1. The quality evaluation for the Pansharpened results on Fig. 2 images.

Fusion Methods	RG-based common fusion quality evaluation criteria (QRG)				
	SAM	SSIM	CC	UQI	RMSE
Our method	**4.8822**	0.7268	0.9668	**0.1286**	**21.3247**
IHS	5.9972	0.7051	0.9658	0.1215	29.9091
Brovey	6.0600	0.7080	0.9660	0.1218	29.8566
PCA	5.9691	0.7151	**0.9689**	0.1222	29.5245
PRACS	6.3753	**0.7434**	0.9597	0.1187	30.6458
BDSD	6.4850	0.6975	0.9586	0.1133	32.9593
ATWT	5.8846	0.7412	0.9648	0.1135	31.5328
AWLP	5.9028	0.7413	0.9645	0.1136	31.4874
MTF_GLP	5.9734	0.7323	0.9644	0.1122	32.1745
MTF_GLP_CBD	6.8192	0.7069	0.9585	0.1066	35.4460
NIHS	6.9245	0.7235	0.9499	0.1209	30.8633
MF	6.4577	0.7191	0.9598	0.1101	32.4162

TABLE 2. The quality evaluation for the Pansharpened results on Fig. 3 images.

Fusion Methods	RG-based common fusion quality evaluation criteria (QRG)				
	SAM	SSIM	CC	UQI	RMSE
Our method	**4.6162**	**0.8062**	0.9514	**0.1884**	**12.6832**
IHS	6.0776	0.7819	0.9476	0.1823	28.6986
Brovey	6.1121	0.7841	0.9485	0.1826	28.8091
PCA	6.0802	0.7912	**0.9536**	0.1844	28.4468
PRACS	7.0768	0.7566	0.9251	0.1752	30.4695
BDSD	6.6703	0.7761	0.9357	0.1675	31.3827
ATWT	7.1926	0.7957	0.9185	0.1670	31.6511
AWLP	7.1921	0.7956	0.9186	0.1669	31.6189
MTF_GLP	7.2986	0.7880	0.9169	0.1665	31.8779
MTF_GLP_CBD	7.4378	0.7745	0.9179	0.1611	32.5460
NIHS	8.0476	0.7109	0.9045	0.1814	31.3062
MF	7.3206	0.7862	0.9212	0.1625	31.2729

B. OBJECTIVE COMPARISON

For the result comparison of different panshapening algorithms, there exist limited accurate quality assessment criteria. It has been proven that the evaluation using consistency properties is reliable for full resolution data experiments [42]. Considering that the recent the radiometric and geometric (RG) scheme [43] segments fused image in edge component with high-frequency and geometric signals and background component with radiometric and spectral information, which well fits our pure and mixed partition idea, we use RG-based common existing criteria to evaluate the performance objectively.

The computation of RG index is performed in two parts of geometric component and radiometric component by a mask of PAN edge map. The edge information from both the PAN and the fused image is used to evaluate the geometric component of the fused image. By subtracting geometric component from fused image, radiometric component is compared between fused image and MS image. To make the RG index in a unique value (QRG), these two components are weighted according to the ratio factor of pixel number in edge section and background section. In this manner, the common indices are calculated in QRG -based scheme.

To validate our method, the results are quantified in terms of spectral angle mapper (SAM), structural similarity (SSIM), correlation coefficient (CC), universal quality index (UQI), root mean square error (RMSE). Obviously, the highest performance of fusion method can obtain small to

TABLE 3. The quality evaluation for the 4-band Pansharpened results on GeoEye-1 dataset in Fig. 2.

Fusion Methods	RG-based common fusion quality evaluation criteria (QRG)				
	SAM	SSIM	CC	UQI	RMSE
Our method	**3.0112**	0.7675	0.9847	**0.1244**	**31.2245**
IHS	4.8754	0.7500	0.9847	0.1203	34.8792
Brovey	4.8754	0.7500	0.9847	0.1203	34.8792
PCA	4.8642	0.7495	**0.9848**	0.1204	34.8607
PRACS	5.1036	**0.7931**	0.9763	0.1176	35.7393
BDSD	4.3849	0.7203	0.9782	0.1086	38.3403
ATWT	4.4348	0.7474	0.9809	0.1102	37.2000
AWLP	4.4453	0.7448	0.9807	0.1101	37.2563
MTF_GLP	4.5936	0.7344	0.9791	0.1086	38.0782
MTF_GLP_CBD	5.8679	0.6704	0.9673	0.1019	42.2484
NIHS	5.5684	0.7792	0.9694	0.1198	35.8688
MF	5.3276	0.7196	0.9724	0.1072	38.1338

TABLE 4. The quality evaluation for the 4-band Pansharpened results on GeoEye −1 dataset in Fig. 3.

Fusion Methods	RG-based common fusion quality evaluation criteria (QRG)				
	SAM	SSIM	CC	UQI	RMSE
Our method	**2.6390**	**0.8426**	**0.9754**	**0.1817**	**19.1719**
IHS	5.3062	0.8122	**0.9754**	0.1756	39.9104
Brovey	5.3062	0.8122	**0.9754**	0.1756	39.9104
PCA	6.3030	0.7748	0.9435	0.1656	40.7585
PRACS	6.1968	0.7671	0.9483	0.1689	41.6754
BDSD	4.3418	0.8068	0.9743	0.1542	42.2135
ATWT	5.5540	0.7790	0.9567	0.1542	42.6864
AWLP	5.5727	0.7737	0.9564	0.1531	42.8422
MTF_GLP	5.7248	0.7679	0.9537	0.1534	43.0261
MTF_GLP_CBD	6.3527	0.7147	0.9447	0.1436	44.9998
NIHS	6.6302	0.7515	0.9449	0.1752	41.5967
MF	6.0200	0.7649	0.9513	0.1493	42.5690

zero for SAM and RMSE, while the other items, i.e., SSIM, CC, and UQI tend to one.

Table 1 and 2 illustrate the performance of RGB image in Fig. 2 and Fig.3, and Table 3 and Table 4 record the quality assessment of 4-band pansharpening results, in which the values representing better performance are in bold for easy observation. From the results in Table 1∼4, we can conclude that our method is better and more reasonable than the other methods in three facts:

1) Higher structure remaining from PAN image in SSIM index, i.e., it employs structure-driven analysis to aid the fused structure synthesis at edge mixed pixels.

2) Better performance in the overall RG index, i.e., our method keeps higher final quality assessment. In CC, the PCA method shows a litter superior performance than our PBSA-based method, since it gets radiometric signal holding from upsampled MS image.

3) Robust for multiple bands. No matter the number of spectral bands changes is 3 or 4, our PBSA-based method keeps higher performance in the overall RG index.

From the visual and objective compared analysis, we can notice that the structure-based pansharpening is attractive in remaining structure of PAN image, constructing spectral signal for interpolated pixels, and fitting different number of multiple spectral bands.

IV. CONCLUSION

In this paper, we have presented a structure-driven spectral mapping from LRMS image to PAN image. This method is based on the partition of PAN blocks and LRMS pixels into pure and mixed classes. We are sure that this is an advocated

earlier to estimate the spectral information considering not only simple MS interpolation but also the guidance of PAN structure. The novel structure analysis aids the distinguished spectral mapping strategy design for different pixel categories. To reduce the spatial information influence of spectral mapping, a simple intensity modification is finally applied to HRMS with reference to PAN. The experimental results on practical remote sensing PAN and LRMS image pairs demonstrate the effectiveness of our PBSA-based method. Compared with the existing pansharpening methods, our structure-driven PBSA-based method has superiority in geometric remaining and radiometric construction for different multiple bands. Therefore, our method retains more accurate spectral information and avoids artificial effects. Because of the pixel classifying, our PBSA-based method takes more time than simple CS-based methods. In the future, we can make some improvements in the program implement to speed up our PBSA-based method.

REFERENCES

[1] C. Thomas, T. Ranchin, L. Wald, and J. Chanussot, "Synthesis of multispectral images to high spatial resolution: A critical review of fusion methods based on remote sensing physics," *IEEE Trans. Geosci. Remote Sens.*, vol. 46, no. 5, pp. 1301–1312, May 2008.

[2] J. R. Kaufman, M. T. Eismann, and M. Celenk, "Assessment of spatial–spectral feature-level fusion for hyperspectral target detection," *IEEE J. Sel. Topics Appl. Earth Observ. Remote Sens.*, vol. 8, no. 6, pp. 2534–2544, Jun. 2015.

[3] J. K. Gilbertson, J. Kemp, and A. van Niekerk, "Effect of pan-sharpening multi-temporal Landsat 8 imagery for crop type differentiation using different classification techniques," *Comput. Electron. Agricult.*, vol. 134, pp. 151–159, Mar. 2017.

[4] K. R. Rahaman, Q. K. Hassan, and M. R. Ahmed, "Pan-sharpening of Landsat-8 images and its application in calculating vegetation greenness and canopy water contents," *ISPRS Int. J. Geo-Inf.*, vol. 6, no. 6, p. 168, 2017.

[5] J. Duran, A. Buades, B. Coll, C. Sbert, and G. Blanchet, "A survey of pansharpening methods with a new band-decoupled variational model," *ISPRS J. Photogramm. Remote Sens.*, vol. 125, pp. 78–105, Mar. 2017.

[6] G. Vivone *et al.*, "A critical comparison among pansharpening algorithms," *IEEE Trans. Geosci. Remote Sens.*, vol. 53, no. 5, pp. 2565–2586, May 2015.

[7] B. Aiazzi, L. Alparone, S. Baronti, A. Garzelli, and M. Selva, "25 years of pansharpening: A critical review and new developments," in *Signal and Image Processing for Remote Sensing*, 2nd ed., C.-H. Chen, Ed. Boca Raton, FL, USA: CRC Press, 2012, pp. 533–548.

[8] W. J. Carper, T. M. Lillesand, and P. W. Kiefer, "The use of intensity-hue-saturation transformations for merging SPOT panchromatic and multispectral image data," *Photogramm. Eng. Remote Sens.*, vol. 56, no. 4, pp. 459–467, Apr. 1990.

[9] P. S. Chavez, Jr., S. C. Sides, and J. A. Anderson, "Comparison of three different methods to merge multiresolution and multispectral data: Landsat TM and SPOT panchromatic," *Photogramm. Eng. Remote Sens.*, vol. 57, no. 3, pp. 295–303, 1991.

[10] T.-M. Tu, S.-C. Su, H.-C. Shyu, and P. S. Huang, "A new look at IHS-like image fusion methods," *Inf. Fusion*, vol. 2, no. 3, pp. 177–186, Sep. 2001.

[11] M. Choi, "A new intensity-hue-saturation fusion approach to image fusion with a tradeoff parameter," *IEEE Trans. Geosci. Remote Sens.*, vol. 44, no. 6, pp. 1672–1682, Jun. 2006.

[12] T.-M. Tu, P. S. Huang, C.-L. Hung, and C.-P. Chang, "A fast intensity-hue-saturation fusion technique with spectral adjustment for IKONOS imagery," *IEEE Geosci. Remote Sens. Lett.*, vol. 1, no. 4, pp. 309–312, Oct. 2004.

[13] T. M. Tu, W. C. Cheng, C. P. Chang, P. S. Huang, and J. C. Chang, "Best tradeoff for high-resolution image fusion to preserve spatial details and minimize color distortion," *IEEE Geosci. Remote Sens. Lett.*, vol. 4, no. 2, pp. 302–306, Apr. 2007.

[14] M. Ghahremani and H. Ghassemian, "Nonlinear IHS: A promising method for pan-sharpening," *IEEE Geosci. Remote Sens. Lett.*, vol. 13, no. 11, pp. 1606–1610, Nov. 2016.

[15] S. Rahmani, M. Strait, D. Merkurjev, M. Moeller, and T. Wittman, "An adaptive IHS pan-sharpening method," *IEEE Geosci. Remote Sens. Lett.*, vol. 7, no. 4, pp. 746–750, Oct. 2010.

[16] M. Cetin and A. Tepecik, "Intensity–hue–saturation-based image fusion using iterative linear regression," *J. Appl. Remote Sens.*, vol. 10, no. 4, p. 045019, Oct. 2016.

[17] Y. Leung, J. Liu, and J. Zhang, "An improved adaptive intensity–hue–saturation method for the fusion of remote sensing images," *IEEE Geosci. Remote Sens. Lett.*, vol. 11, no. 5, pp. 985–989, May 2014.

[18] M. González-Audícana, J. L. Saleta, R. G. Catalán, and R. García, "Fusion of multispectral and panchromatic images using improved IHS and PCA mergers based on wavelet decomposition," *IEEE Trans. Geosci. Remote Sens.*, vol. 42, no. 6, pp. 1291–1299, Jun. 2004.

[19] V. P. Shah, N. H. Younan, and R. L. King, "An efficient pan-sharpening method via a combined adaptive PCA approach and contourlets," *IEEE Trans. Geosci. Remote Sens.*, vol. 46, no. 5, pp. 1323–1335, May 2008.

[20] B. Aiazzi, S. Baronti, and M. Selva, "Improving component substitution pansharpening through multivariate regression of MS+Pan data," *IEEE Trans. Geosci. Remote Sens.*, vol. 45, no. 10, pp. 3230–3239, Oct. 2007.

[21] R. Restaino, M. D. Mura, G. Vivone, and J. Chanussot, "Context-adaptive pansharpening based on image segmentation," *IEEE Trans. Geosci. Remote Sens.*, vol. 55, no. 2, pp. 753–766, Feb. 2017.

[22] D. A. Yocky, "Multiresolution wavelet decomposition image merger of Landsat thematic mapper and SPOT panchromatic data," *Photogramm. Eng. Remote Sens.*, vol. 62, no. 9, pp. 1067–1074, 1996.

[23] J. Zhou, D. L. Civco, and J. A. Silander, "A wavelet transform method to merge Landsat TM and SPOT panchromatic data," *Int. J. Remote Sens.*, vol. 19, no. 4, pp. 743–757, 1998.

[24] P. Scheunders and S. De Backer, "Fusion and merging of multispectral images with use of multiscale fundamental forms," *J. Opt. Soc. Amer. A, Opt. Image Sci.*, vol. 18, no. 10, pp. 2468–2477, Oct. 2001.

[25] A. Garzelli and F. Nencini, "PAN-sharpening of very high resolution multispectral images using genetic algorithms," *Int. J. Remote Sens.*, vol. 27, no. 15, pp. 3273–3292, 2006.

[26] I. Amro, J. Mateos, M. Vega, R. Molina, and A. K. Katsaggelos, "A survey of classical methods and new trends in pansharpening of multispectral images," *EURASIP J. Adv. Signal Process.*, vol. 2011, no. 1, pp. 1–22, Sep. 2011.

[27] F. Nencini, A. Garzelli, S. Baronti, and L. Alparone, "Remote sensing image fusion using the curvelet transform," *Inf. Fusion*, vol. 8, no. 2, pp. 143–156, 2007.

[28] B. Aiazzi, L. Alparone, S. Baronti, and A. Garzelli, "Context-driven fusion of high spatial and spectral resolution images based on oversampled multiresolution analysis," *IEEE Trans. Geosci. Remote Sens.*, vol. 40, no. 10, pp. 2300–2312, Oct. 2002.

[29] B. Aiazzi, L. Alparone, S. Baronti, A. Garzelli, and M. Selva, "MTF-tailored multiscale fusion of high-resolution MS and Pan imagery," *Photogramm. Eng. Remote Sens.*, vol. 72, no. 5, pp. 591–596, May 2006.

[30] L. Alparone, L. Wald, J. Chanussot, C. Thomas, P. Gamba, and L. M. Bruce, "Comparison of pansharpening algorithms: Outcome of the 2006 GRSS data fusion contest," *IEEE Trans. Geosci. Remote Sens.*, vol. 45, no. 10, pp. 3012–3021, Oct. 2007.

[31] A. Garzelli, F. Nencini, and L. Capobianco, "Optimal MMSE pan sharpening of very high resolution multispectral images," *IEEE Trans. Geosci. Remote Sens.*, vol. 46, no. 1, pp. 228–236, Jan. 2008.

[32] S. Zhong, Y. Zhang, Y. Chen, and D. Wu, "Combining component substitution and multiresolution analysis: A novel generalized BDSD pansharpening algorithm," *IEEE J. Sel. Topics Appl. Earth Observ. Remote Sens.*, vol. 10, no. 6, pp. 2867–2875, Jun. 2017.

[33] C. Jiang, H. Zhang, H. Shen, and L. Zhang, "Two-step sparse coding for the pan-sharpening of remote sensing images," *IEEE J. Sel. Topics Appl. Earth Observ. Remote Sens.*, vol. 7, no. 5, pp. 1792–1805, May 2014.

[34] M. Guo, H. Zhang, J. Li, L. Zhang, and H. Shen, "An online coupled dictionary learning approach for remote sensing image fusion," *IEEE J. Sel. Topics Appl. Earth Observ. Remote Sens.*, vol. 7, no. 4, pp. 1284–1294, Apr. 2014.

[35] H. Yin, "A joint sparse and low-rank decomposition for pansharpening of multispectral images," *IEEE Trans. Geosci. Remote Sens.*, vol. 55, no. 6, pp. 3545–3557, Jun. 2017.
[36] G. Masi, D. Cozzolino, L. Verdoliva, and G. Scarpa, "CNN-based pan-sharpening of multi-resolution remote-sensing images," in *Proc. Joint Urban Remote Sens. Event*, Mar. 2017, pp. 1–4.
[37] Y. Wei and Q. Yuan, "Deep residual learning for remote sensed imagery pansharpening," in *Proc. IEEE Int. Workshop Remote Sens. Intell. Process.*, May 2017, pp. 1–4.
[38] L. Loncan *et al.*, "Hyperspectral pansharpening: A review," *IEEE Trans. Geosci. Remote Sens.*, vol. 3, no. 3, pp. 27–46, Sep. 2015.
[39] B. Alexe, T. Deselaers, and V. Ferrari, "What is an object?" in *Proc. IEEE Conf. Comput. Vis. Pattern Recognit.*, Jun. 2010, pp. 73–80.
[40] R. Restaino, G. Vivone, M. Dalla Mura, and J. Chanussot, "Fusion of multispectral and panchromatic images based on morphological operators," *IEEE Trans. Image Process.*, vol. 25, no. 6, pp. 2882–2895, Jun. 2016.
[41] *Quality Assessment RG Index*. Accessed: Jul. 14, 2017. [Online]. Available: http://openremotesensing.net/knowledgebase/quality-assessment-of-pan-sharpening-methods-in-high-resolution-satellite-images-using-radiometric-and-geometric-index/
[42] F. Palsson, J. R. Sveinsson, M. O. Ulfarsson, and J. A. Benediktsson, "Quantitative quality evaluation of pansharpened imagery: Consistency versus synthesis," *IEEE Trans. Geosci. Remote Sens.*, vol. 54, no. 3, pp. 1247–1259, Mar. 2016.
[43] M. Hasanlou and M. R. Saradjian, "Quality assessment of pan-sharpening methods in high-resolution satellite images using radiometric and geometric index," *Arabian J. Geosci.*, vol. 9, no. 1, p. 45, Jan. 2016.

XIAOYAN LUO (M'12) received the B.S. degree in communication engineering from the Taiyuan University of Technology, Taiyuan, Shanxi, China, in 2004, and the M.S. and Ph.D. degrees from Beihang University, Beijing, China, in 2007 and 2012, respectively.

She is currently a Lecturer with the Image Processing Center, Beihang University. Her research interests include image fusion, computer vision, and hyperspectral image processing.

LIANGYU ZHOU received the B.S. degrees from Beihang University, Beijing, China, in 2016, where he is currently pursuing the M.S. degree with the School of Astronautics.

His research interests include image fusion, sparse representation, and dictionary learning.

XIAOFENG SHI is currently an Associate Professor with the School of Electronics and Information Engineering, Beihang University.

His research interests include signal processing, aviation navigation, flight inspection, measurement, and control technology.

HAN WAN is currently a Lecturer of computer science and engineering with Beihang University.

She has also led research projects on innovations in pedagogy, curriculum, and educational technology. Her research includes computer architecture simulation, WCET analysis in real-time system, parallel computing, and GPU accelerating general purpose application.

JIHAO YIN (M'10–SM'15) received the Ph.D. degree from the Beijing Institute of Technology, Beijing, China, in 2007. He is with Beihang University, Beijing, where he is currently an Associate Professor with the Image Processing Center, School of Astronautics. From 2015 to 2017, he was a Visiting Scientist with the Department of Electrical Engineering and Computer Science, Massachusetts Institute of Technology, Cambridge, MA, USA. He has authored over 50 research papers. His current research interests include image processing and remote sensing applications.